https://doi.org/10.5194/egusphere-2026-3281
Preprint. Discussion started: 24 June 2026

Machine-learning projections of boreal forest gross primary productivity under future climate change

Sandip V George[1], Cameron F. T. Pope[1], Stella Jes Varghese[2], and Ron Sunny[3]

[1]Department of Physics, University of Aberdeen, United Kingdom
[2]Centre for Climate Change, Atria University, ASKB Campus, Hebbal, Bengaluru, India
[3]National Centre for Biological Sciences (NCBS), Bangalore, India

Correspondence: Sandip V George (sandip.george@abdn.ac.uk)

Abstract. Modelling forest productivity under climate variability and change remains a key challenge in terrestrial ecology. The increasing availability of long-term eddy covariance data enables these relationships to be explored using data-driven machine-learning approaches. In this study, we model the relationship between four key environmental variables, namely, photosynthetically active radiation (PAR), atmospheric CO_2 concentration, air temperature, and relative humidity, and gross primary productivity (GPP) using linear regression, eXtreme Gradient Boosting (XGBoost), and deep neural networks. To capture variability across temporal scales, the input variables are decomposed into trend, seasonal, and residual components representing long-term, seasonal, and inter-daily fluctuations. The models are trained on seventeen years (2003–2019) of daily observations from the boreal forest monitoring station at Hyytiälä, Finland, and evaluated on an independent five-year period (2020–2025). The trained models are then used to project GPP under four Shared Socioeconomic Pathway (SSP) scenarios from the Intergovernmental Panel on Climate Change using climate forcings derived from Coupled Model Intercomparison Project Phase 6 (CMIP6) simulations.

All models show strong predictive skill (R^2=0.79–0.90; RMSE =1.03–1.49), with the DNN performing best overall. SHAP (SHapley Additive exPlanations) analysis identifies the residual component of PAR as the most influential predictor of GPP across all models. More broadly, residual components across multiple inputs show high predictive importance, suggesting that short-term variability in environmental conditions may play an important role in explaining modeled GPP fluctuations. Projections driven by an ensemble of four CMIP6 climate models suggest relatively stable GPP during the mid-century period across SSP scenarios, followed by an overall increase toward the end of the century, particularly under higher-emission pathways. Overall, this study demonstrates the potential of combining long-term ecosystem observations, engineered environmental features, and climate-model projections to generate localized forecasts of forest productivity. However, we highlight the need for cautious interpretation of these results, since these are data-driven models that are being extrapolated beyond historical climate conditions

1 Introduction

Forests play an integral role in regulating the global carbon cycle, but their distribution and functioning are increasingly being altered by climate change. Understanding how forest ecosystems interact with the atmosphere, and how these interactions

https://doi.org/10.5194/egusphere-2026-3281
Preprint. Discussion started: 24 June 2026

may shift under future climatic conditions, is therefore critical for predicting forest responses to global change(Keenan et al., 2015; Graham et al., 1990; Walker and Kasting, 1992; Kafy et al., 2023). However, links between atmospheric conditions and local ecosystem functioning remain difficult to resolve because they are complex, nonlinear and shaped by multiple interacting climatic drivers. A key question is how variation in atmospheric conditions influences biomass production through photosynthesis. This ecosystem-level carbon uptake is commonly quantified as gross primary productivity (GPP), defined as the total amount of carbon fixed by photosynthesis within an ecosystem over a given period (Ashton et al., 2012).

Although it is well understood that GPP has increased in recent decades, especially in the northern higher latitudes, the mechanism behind this is less understood(Ahlström et al., 2015; Pysarenko et al., 2022; Keenan et al., 2016; Fernández-Martínez et al., 2017). While rising CO_2 concentration in the atmosphere due to emissions is a contributing factor, the extent of its contribution is a subject of debate. Other possible contributing factors include rising air temperatures, increased atmospheric nitrogen deposition, increased light availability and biophysical factors(Keenan et al., 2016; de Vries et al., 2014; Mercado et al., 2009; Launiainen et al., 2022). Disentangling these various factors, and their contributions to GPP is crucial to understand how forests will behave in response to different climate scenarios.

The dependence of GPP on these variables can be studied using various modelling approaches including biophysics based models such as the Atmosphere-Plant Exchange Simulator (APES) (Launiainen et al., 2015), time series models such as ARIMA (Bo et al., 2022) and modified vector autoregressive(VAR) models (Green et al., 2017), as well as machine learning methods such as support vector machines (SVM), random forests, feedforward neural networks and recurrent neural networks (RNNs)(Yang et al., 2007; Ezhova et al., 2025; Zhu et al., 2020; Agarwal et al., 2023; Montero et al., 2024; Agarwal et al., 2024). While biophysical models have a major advantage of being based on theory, when used for predictions, they are susceptible to inaccuracies in model assumptions. Time series models, including machine learning models such as RNNs are excellent for short term predictions, but the prediction errors increase as the model predicts further in time. Feature-based models, such as linear regression, random forests and feed forward neural networks, are better suited for long term predictions, particularly when considering responses in GPP under predicted climate scenarios (Lu et al., 2024; Sarkar et al., 2022).

Testing ML models trained on historical data provides a promising pathway for evaluating future forest dynamics. The Coupled Model Intercomparison Project Phase 6 (CMIP6) provides standardized high resolution climate simulations and future climate projections, which can serve as driving variables in our machine learning models. By forcing our machine learning models with CMIP6 derived data, we bypass the uncertainty arising from error-propagation that is inherent in recursive time series forecasting. Moreover, CMIP6 provides a range of possible future scenarios, where-from we can derive reliable information about future climate state. Hence, we develop an approach that projects GPP as a function of environmental drivers rather than time, providing a more stable lens through which to view ecosystem responses to various Shared Socioeconomic Pathways (SSPs). Although training on historical SMEAR II data and applying the models to CMIP6 climate projections introduces potential risks associated with distribution shift and overfitting, machine learning models such as Random Forests and neural networks can capture complex nonlinear interactions within the observed data. Their application to CMIP6 forcing therefore provides a useful, though uncertain, framework for exploring ecosystem responses under projected future climate conditions.

https://doi.org/10.5194/egusphere-2026-3281
Preprint. Discussion started: 24 June 2026

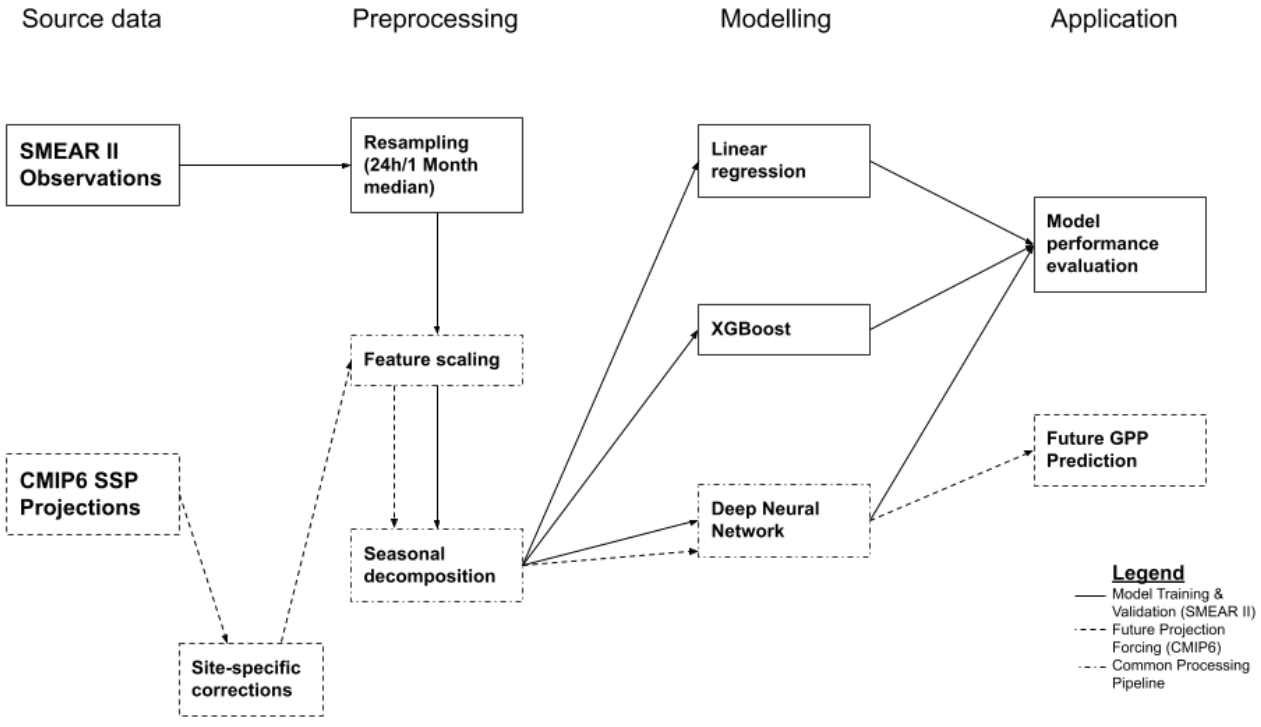

Figure 1. Methodological framework for GPP modelling and future projection. The workflow illustrates the parallel processing of historical observations (SMEAR II, solid lines) and future climate projections (CMIP6, dashed lines). Both datasets undergo common preprocessing steps (dash-dotted lines), including temporal resampling and seasonal decomposition. Following model training and performance evaluation on historical data, the optimized architectures are forced with CMIP6 data to generate GPP projections for 2040–2050.

2 Data and Methods

In the following sections, we describe the data, the preprocessing steps involved and the models that were used for analysis. All the analysis was conducted in python v 3.11.3, and our full pipeline is shown in the flowchart in Figure 1.

https://doi.org/10.5194/egusphere-2026-3281
Preprint. Discussion started: 24 June 2026

2.1 Data

Data were obtained from the Station for Measuring Ecosystem-Atmospheric Relations (SMEAR-II) located in Hyytiälä, Finland, 200 kilometers north-west of Helsinki (61.85° N, 24.29° E) (inset of Figure 2). It is operated by the University of Helsinki and is the second of such stations, often referred to as SMEAR-II or the SMEAR flagship. It consists of a 128 meter tall measurement mast and measurement towers within and above the tree canopy, which continuously monitors forest ecophysiology and productivity, soil and water balance, meteorology, solar and terrestrial radiation, fluxes, ambient concentrations, atmospheric aerosols and deposition(Hari et al., 2013). The SMEAR II station is situated in a homogeneous Scots pine boreal forest. Boreal forests constitute up to 30% of the Earth's land surface area, meaning the results obtained can be interpreted and used as a representation of other, similar, forestland(Gauthier et al., 2015). The station has been operational since 1995 and continuously records over 1200 variables, the majority of which are measured every minute. 20 years of data, spanning 1 January 2003 to 31 December 2025 were obtained using the smart-SMEAR tool, with hourly averages calculated using the arithmetic mean (Junninen et al., 2009). The Hyytiälä site was significantly thinned in 2019, with a removal of about 30% of the tree basal area(Juho et al., 2023). Our dataset spans both pre- and post-thinning conditions at the site. Because the models used in this study do not explicitly consider temporal aspects or regime shifts, ignoring this distinction likely increases variability in the data.

Our main variable of interest, the GPP, is derived using the eddy covariance technique as detailed in (Kulmala et al., 2019). We chose GPP as our target variable instead of Net Ecosystem Exchange (NEE) because it more directly reflects canopy photosynthetic activity, without the combined influence of autotrophic and heterotrophic respiration present in NEE. This facilitates the analysis of growing season dynamics and potential CO_2 fertilization responses, while avoiding the larger uncertainties often associated with nighttime NEE measurements under stable atmospheric conditions (Loescher et al., 2006).

2.1.1 Predictor variables

The predictors for our model were chosen based on three criteria (i) the variables are known to correlate with GPP, as this will allow the models to have more statistical power when predicting future values for GPP, (ii) the variables are expected to change as a result of climate change and (iii) the variables were readily available in the dataset. On this basis, Photosynthetically active radiation (PAR), CO_2 concentration (CO_2), relative humidity (RH) and air temperature (AT) were chosen. All of these variables are known to influence photosynthesis. PAR, which represents the part of sunlight that can be used for photosynthesis, is the primary driver of photosynthesis. RH is indirectly related to photosynthetic activity, influencing transpiration rate and stomatal closures which influence photosynthesis. CO_2 concentration and AT, apart from being important factors for photosynthesis, also are changing rapidly as a result of human activity.

2.1.2 Missing data

To construct a continuous daily time series for the study period, meteorological and flux data from the SMEAR II station were integrated across multiple sensors. For AT, CO_2 and PAR, gaps in the primary station records were filled via linear interpolation

https://doi.org/10.5194/egusphere-2026-3281
Preprint. Discussion started: 24 June 2026

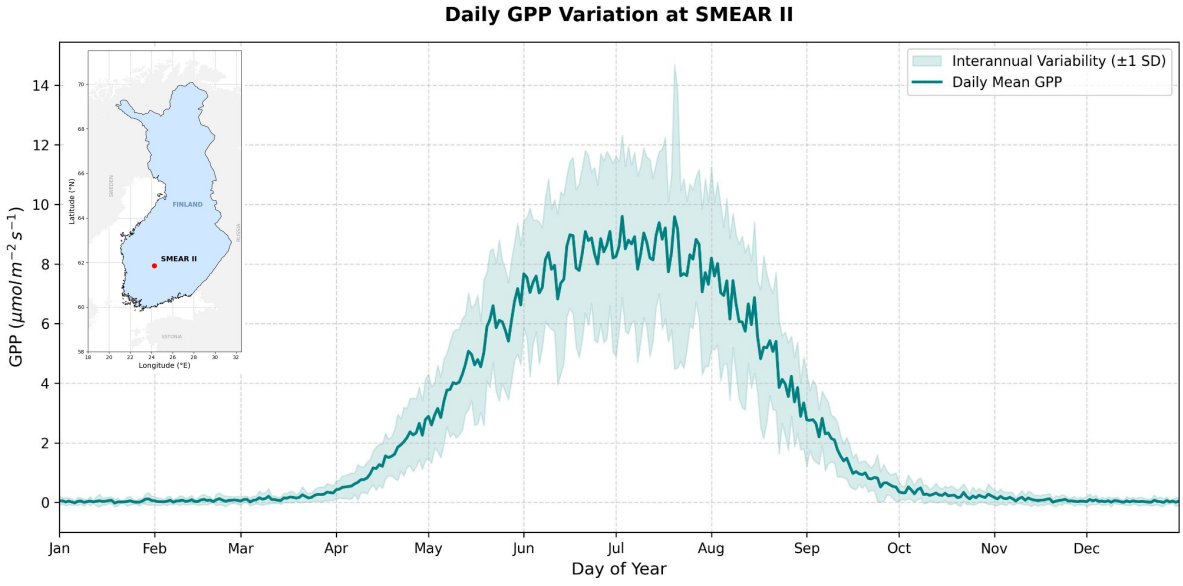

Figure 2. Daily profile of gross primary productivity (GPP) at the SMEAR II station for the study period (2003–2025). The solid line represents the multi-year daily mean, and the shaded ribbon indicates the interannual variability (± 1 standard deviation). The inset shows the location of the SMEAR II site.

using secondary data from non-official ICOS sensors and a Delta-T BF3/BF5 sunshine sensor, respectively. For RH, a change in measurement height from 16 m to 35 m in February 2017 necessitated a systematic homogenization to prevent artificial discontinuities. A transfer-standard approach was employed using an infra-red gas analyzer (IRGA) as a common reference "bridge." Ordinary least squares (OLS) regression models were trained during overlapping periods to relate each primary RH sensor to the IRGA baseline. These models were then used to both fill the 2013–2017 data gap and bias-correct the post-2017 data to a 16 m equivalent baseline. Finally, all variables were aggregated to 24-hour medians and physically constrained to ensure consistency.

2.1.3 Seasonal Decomposition

One major issue in modelling ecological time series is the presence of strong periodicities. In the northern boreal forests where the SMEAR-II monitoring station is located, less than six hours of daylight per day are observed during the winter solstice. Modelling these oscillations can be challenging, as seasonal trends must be separated from longer-term trends associated with climate change. Seasonal variations are present in all of our variables, namely PAR, air temperature (AT), CO_2 concentration, relative humidity (RH), and GPP. In addition, diurnal variations occur to differing degrees in each of these variables. A real danger in this scenario is that the machine learning models may simply learn the seasonal relationships between variables, which are driven primarily by the seasonal cycle in climate, rather than capturing the intrinsic dependence between GPP and the predictor variables. The day-to-day variability of GPP at the SMEAR II site are shown in Figure 2.

https://doi.org/10.5194/egusphere-2026-3281
Preprint. Discussion started: 24 June 2026

To mitigate the risk that the machine learning models learn only the shared seasonal cycle between variables rather than their intrinsic relationships, we preprocess the time series to separate variability occurring across different temporal scales. To remove the effects of diurnal variations, the dataset was first resampled by taking the median within 24-hour windows. Beyond reducing day-level periodicity, this larger window also helps reduce noise in the dataset. To account for yearly and interannual variability, we then applied a classical time-series decomposition based on a moving average to separate each time series into seasonal, trend, and residual components. These components represent seasonal variability, long-term changes, and short-term fluctuations, respectively, effectively partitioning the input variables into three timescales that may influence different aspects of GPP. This decomposition therefore allows us to examine how each variable contributes to seasonal dynamics, long-term climatic effects, and inter-daily variability in GPP. The decomposition was carried out using the `statsmodels` package (Seabold and Perktold, 2010). Further details of the decomposition are provided in Appendix A.

All features were standardized prior to training to ensure zero mean and unit variance, allowing variables to be on a comparable scale and preventing features with larger numerical magnitudes from dominating model training.

2.1.4 Future climate projections

To evaluate GPP under future climate conditions, we utilized daily bias-corrected and statistically downscaled projections from the NASA Earth Exchange Global Daily Downscaled Projections (NEX-GDDP-CMIP6) dataset. The analysis incorporates outputs from four models, namely EC-Earth3, CESM2, CNRM-CM6-1-HR, and NorESM2-LM(Thrasher et al., 2022). The dataset employs the Bias-Correction and Spatial Disaggregation (BCSD) method to perform bias correction and statistical downscaling of CMIP6 outputs, resulting in a gridded product at $0.25^\circ \times 0.25^\circ$ spatial resolution for the period 1980-2100. We extracted data for the 0.25° grid cell encompassing the SMEAR II station coordinates. To provide a comprehensive range of potential climate trajectories, we selected Tier 1 scenarios from the CMIP6 ScenarioMIP(O'Neill et al., 2016; Tebaldi et al., 2021) encompassing four Shared Socioeconomic Pathways (SSPs): SSP1-2.6 (low emissions), SSP2-4.5 (intermediate emissions), SSP3-7.0 (high-middle), and SSP5-8.5 (high emissions).

Our reduced CMIP6 ensemble was selected to balance structural diversity, regional relevance, and computational tractability. Following performance-based sub-selection principles for European impact studies (Palmer et al., 2023), we prioritized models from independent modeling centres and distinct model lineages rather than relying on a single model or the full ensemble. Model choice was further informed by published evaluations of CMIP6 surface down-welling shortwave radiation, since radiation is a key driver of ecosystem productivity in our framework (He et al., 2023). The final subset (EC-Earth3, CESM2, CNRM-CM6-1-HR, and NorESM2-LM) therefore samples a range of plausible climate responses while avoiding obvious redundancy, with NorESM2-LM additionally included for its relevance to high-latitude and Nordic climates.

While the NEX-GDDP-CMIP6 dataset provides daily outputs for most meteorological variables, CO_2 concentration from the input4MIPs dataset is only available at monthly resolution. To ensure consistency across all forcing variables, the modelling framework was therefore implemented at a monthly temporal scale.. Consequently, future projections were conducted at a monthly temporal scale. For these projections, the best-performing architecture (the Deep Neural Network) was retrained using monthly-aggregated SMEAR II data before being forced with the CMIP6 ensemble outputs.

https://doi.org/10.5194/egusphere-2026-3281
Preprint. Discussion started: 24 June 2026

Although the NEX-GDDP dataset is bias-corrected relative to global products, local atmospheric conditions at the boreal forest site required further refinement. We applied a station-specific bias correction by fitting a linear model to the overlapping historical period (2003–2015) between the SMEAR II observations and the CMIP6 historical runs. In particular for PAR, a broken linear model was used, since the PAR derived from the surface downward shortwave radiation from CMIP6 was overestimated in winter and underestimated in summer. These secondary corrections ensure that the driving variables for our machine learning models remain consistent with the unique profile of the Hyytiälä forest (More details can be found in Appendix B).

2.2 Models

We use three models for modelling the relationships between our predictor and outcome variables, namely linear regression, extreme gradient boosting (XGBoost) and a deep neural network. The linear regression model is our baseline, interpretable model, where the relation between the predictor variables and GPP is purely linear. The XGBoost model utilizes an ensemble of gradient-boosted decision trees which captures non-linear interactions between the predictor variables, without the intensive computational requirements of deep learning (Chen and Guestrin, 2016). The Deep Neural Network (DNN) is a multi-layered connectionist model which can provide even greater flexibility by approximating complex, hierarchical relationships between our environmental drivers and GPP (LeCun et al., 2015). Hence, these models represent increasing levels of flexibility and nonlinearity.

2.2.1 Linear regression

For our baseline we choose the linear regression model. It can be written as

$$f(x_i) = c + \sum_i a_i x_i \tag{1}$$

where $f(x_i)$ is the outcome variable, x_is are the predictor variables, a_is are the linear coefficients and c is the intercept. A linear regression model works with the assumption that the relationships between the predictors and outcome are linearly related, an assumption that is violated in this dataset, where GPP is known to have nonlinear relations with the predictors. Hence the results of linear regression serves as a good starting point to measure the improvements offered by other models such as the XGBoost and the deep neural network.

2.2.2 XGBoost

XGBoost is an ensemble method which combines the output from several, individual decision trees in order to create a single output(Chen and Guestrin, 2016). By combining a large number of individual decision trees for a prediction, this can help reduce variability and noise of the output. Unlike a random forest, which uses the output of a number of trees in parallel, XGBoost uses a boosting approach where the decision trees are constructed sequentially, with a subsequent tree correcting the predictions from a previous tree. In gradient boosting, the loss function is minimized using gradient descent resulting in a

https://doi.org/10.5194/egusphere-2026-3281
Preprint. Discussion started: 24 June 2026

faster convergence. In our study XGBoost was used as a regressor, with 1000 decision trees predicting GPP from our feature set. XGBoost allows early termination of training if further improvements to the model are not found and was set to 50 iterations in this case.

2.2.3 Neural Networks

Our final model is a DNN. Neural networks consist of layers of 'neurons' with weighted connections between them. Neural networks consist of an input layer, one or more hidden layers and an output layer. Neural networks are termed deep when they consist of multiple hidden layers. A node is activated when an input to it is above a certain threshold, determined by an activation function.

Our model consisted of a neural network with five hidden layers using Exponential Linear Unit (ELU) activation functions. The first hidden layer contained 64 neurons, with the number of neurons progressively decreasing to 4 in the final hidden layer, followed by a single neuron output layer with a linear activation function. Batch normalization was applied after the first three hidden layers, and L2 regularization was used to reduce overfitting. The neural network was implemented using the Keras library, which provides an interface for TensorFlow (Ketkar and Ketkar, 2017; Abadi et al., 2016). To account for variability arising from random initialization, an ensemble of independently trained networks was used, and projections were summarized using the ensemble median.

Feature importance in all models was assessed using SHAP (SHapley Additive exPlanations) values, which quantify the contribution of each input feature to the model prediction based on cooperative game theory. SHAP values represent the marginal contribution of a feature averaged over all possible combinations of inputs, providing a consistent measure of feature importance for machine learning models. In this study, we report the mean absolute SHAP values, which indicate the overall influence of each feature on the model output.

3 Results

We list out the results of the various models and the corresponding root mean square error (RMSE) values in section 3.1. The first 75% of the data set was used for training (2003- $\approx$ 2020) and the last 25% ($\approx$ 2020-2025) for testing. We also use the neural network model to make predictions of the GPP under future climate scenarios in section 3.2.

3.1 SMEAR II Site Predictions

The baseline linear regression model yielded an R^2 value of 0.79. Predictions on the test set resulted in an RMSE of 1.49 and an MAE value of 1.09. The XGBoost model showed improved predictive performance, with a higher R^2 value of 0.89 and lower RMSE and MAE values of 1.10 and 0.77, respectively, on the test set. Since the deep learning model (DNN) is stochastic in nature, we ran the model five times and took the median prediction across the five runs at each time point. This yielded the highest predictive skill on the test set compared to both linear regression and XGBoost, with $R^2 = 0.90$ and RMSE and MAE

https://doi.org/10.5194/egusphere-2026-3281
Preprint. Discussion started: 24 June 2026

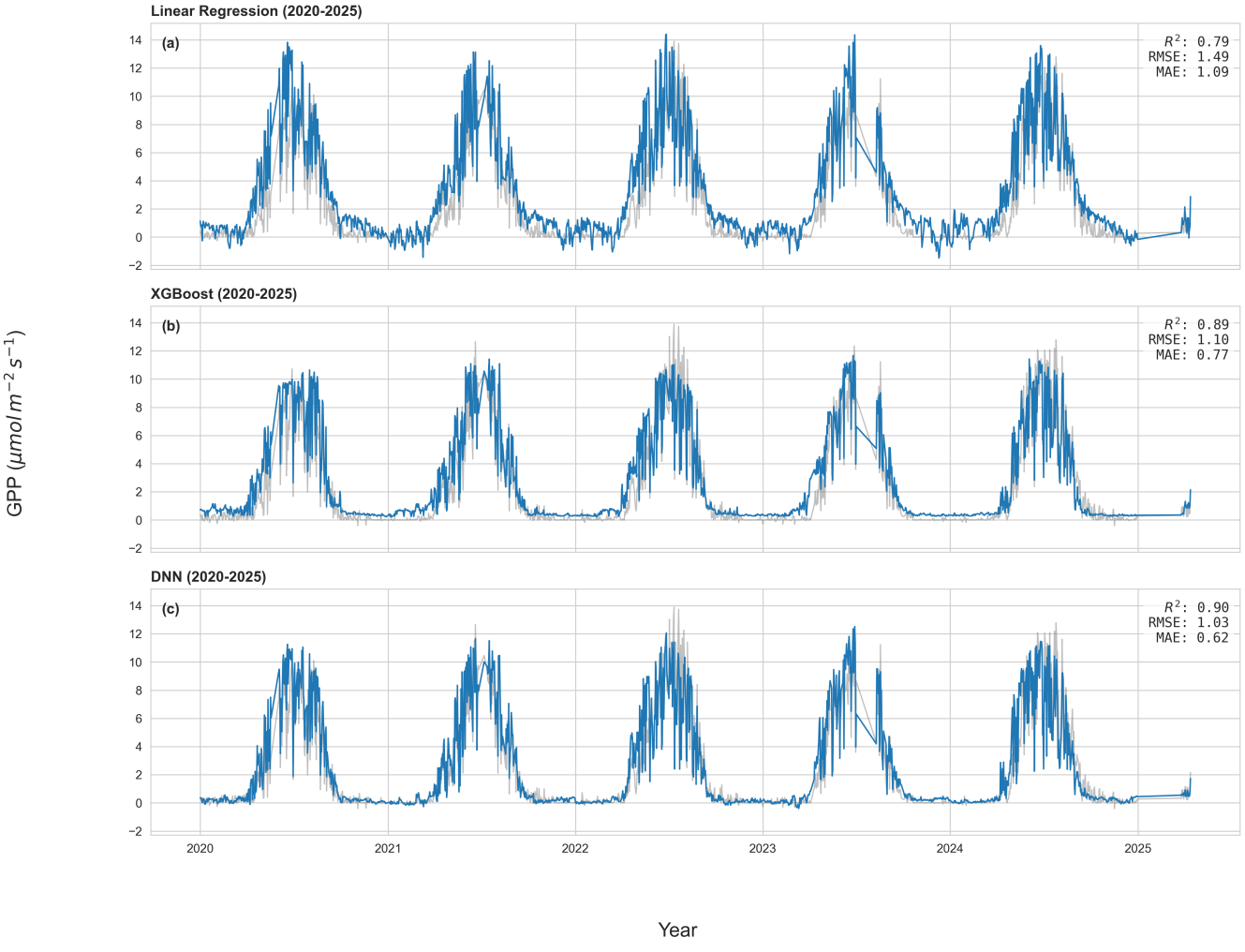

Figure 3. Plot showing the comparative predictions of GPP by (a) linear regression, (b)XGBoost and (c) Deep neural network. The true GPP values are shown in gray in the background of each prediction.

of 1.03 and 0.62. The predictions of the three models and the comparative R^2, RMSE and MAE values are shown in Figure 3. A large part of the 2025 data was lost due to the edge-truncation effects inherent to the seasonal decomposition algorithm.

While the overall performance metrics are informative, they do not provide the full picture. When comparing the observed and predicted time series for each model, the linear regression model tends to overpredict GPP on average, particularly during the winter months. XGBoost also exhibits this tendency, although to a lesser extent. In contrast, the DNN appears to strike a better balance, capturing both winter and summer GPP more effectively.

Although the DNN achieved the highest predictive performance, the differences relative to XGBoost and linear regression were moderate. Notably, the linear regression model was able to capture a substantial fraction of the variance in GPP, indicating

https://doi.org/10.5194/egusphere-2026-3281
Preprint. Discussion started: 24 June 2026

that a large component of the variability can be explained by approximately linear relationships with the environmental drivers. However, differences between the models become more apparent during periods of large fluctuations in the predictor variables.

3.1.1 Feature Importance

We then conducted a feature importance analysis using SHAP values for all three models. The normalized mean absolute SHAP value for the three models is shown in Figure 4. Across all models, the residual component of PAR emerged as the most important feature. For the best-performing DNN model, the seasonal components of PAR and CO_2, along with the residual components of air temperature (AT) and CO_2, were also among the most influential features. Notably, for the DNN, the residual component was the most important contribution within most environmental variables.

This suggests that the models primarily respond to short-term fluctuations in the environmental drivers, rather than relying solely on the shared seasonal cycle or long-term trends. In contrast, the trend components consistently show lower importance across all models, which may reflect the relatively small magnitude of long-term changes over the training period. In particular, the dominance of PAR-related features highlights the primary role of radiation in controlling GPP variability at this site.

3.2 CMIP6 based projections

The DNN, identified as the best-performing architecture, was employed to project GPP trajectories under future climate scenarios. To ensure consistency with the monthly resolution of the CMIP6 climatic drivers and to mitigate the impact of daily-scale stochastic noise absent in the CMIP6 data, the model was retrained using monthly-averaged SMEAR observations. This retrained model maintained robust predictive performance, achieving an R^2 of 0.97 and an RMSE of 0.54 on a held-out test set comprising 10% of the monthly SMEAR II data.

Projections were generated by forcing the trained models with environmental variables derived from four CMIP6 models across four Shared Socioeconomic Pathways (SSPs). These variables were subjected to a site-specific bias correction based on linear models fitted between the historical CMIP6 simulations and the corresponding observations from the SMEAR II site. Details of the correction procedure are provided in Appendix B, while the performance of the corrected historical simulations in reproducing observed GPP is evaluated in Appendix C.

All scenarios indicate an increase in GPP relative to the historical period (Table 1). The temporal evolution of these projections and their associated monthly variability are shown in Figures 5 and 6, respectively. While the projected trajectories remain broadly similar across all SSPs until approximately mid-century, substantial divergence emerges towards the end of the century, with SSP3-7.0 and SSP5-8.5 exhibiting the largest increases in productivity. Examination of the monthly climatologies (Figure 6) suggests that a significant contribution to this divergence arises from increased productivity during the winter months.

https://doi.org/10.5194/egusphere-2026-3281
Preprint. Discussion started: 24 June 2026

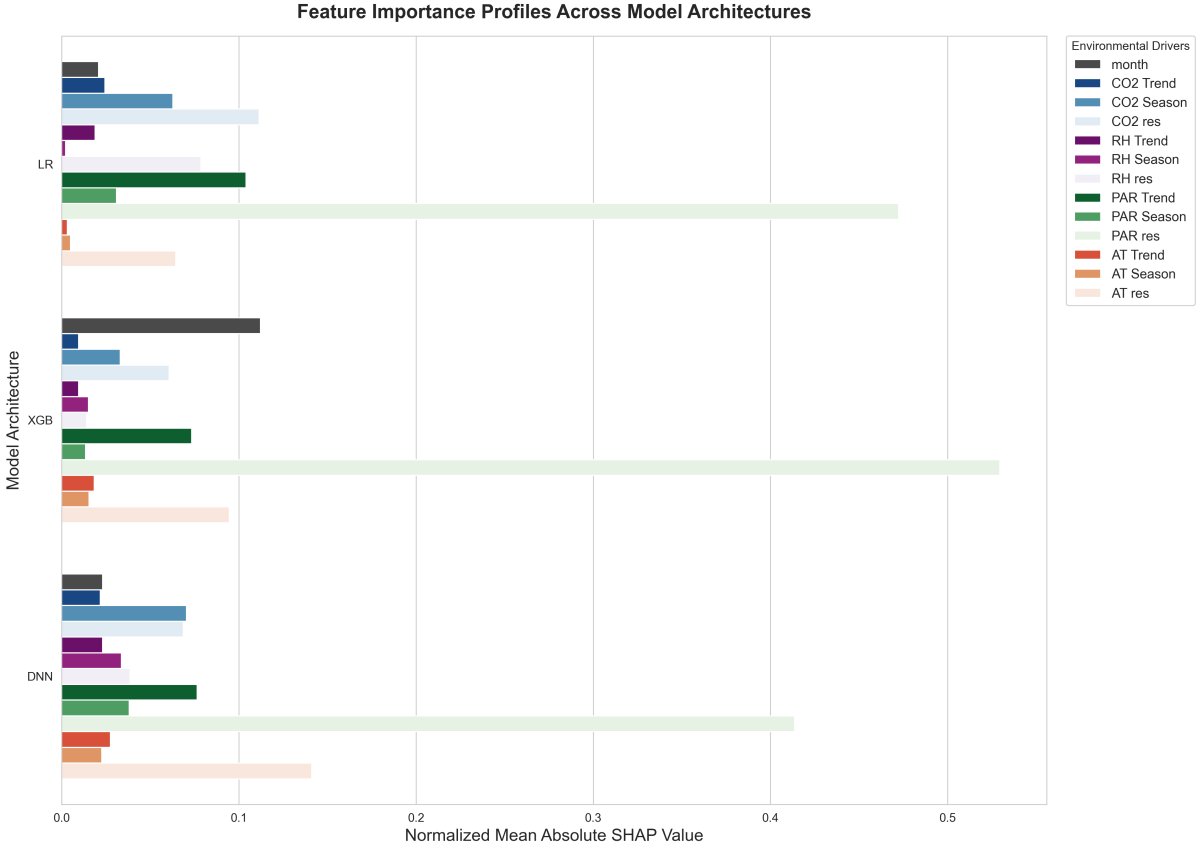

Figure 4. Feature importance scores using a SHAP analysis on the three models used. Season, Trend and Res represent the three components after decomposition of each feature.

SSP	GPP (mid-century)	GPP (end-century)
1-2.6	647.37 ± 284.98	669.47 ± 292.61
2-4.5	641.50 ± 284.98	727.95 ± 320.87
3-7.0	631.04 ± 279.05	1080.41 ± 571.68
5-8.5	674.68 ± 297.64	1527.70 ± 718.10

Table 1. Average projected GPP under different climate scenarios in the mid and end century. The error is the Inter-model standard deviation (Spread). The GPP is measured in $gCm^{-2}yr^{-1}$.

https://doi.org/10.5194/egusphere-2026-3281
Preprint. Discussion started: 24 June 2026

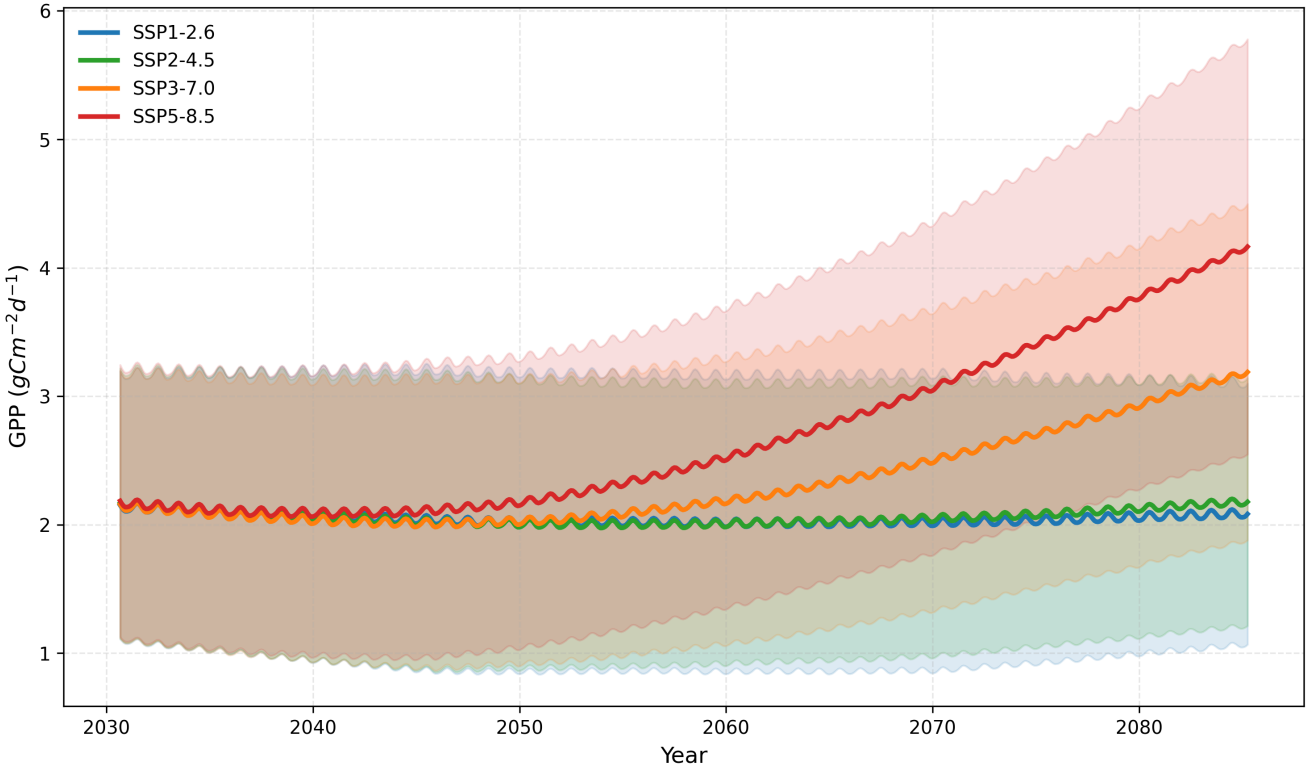

Figure 5. Projected changes of GPP under different CMIP6 SSPs. The bands around the solid lines represent the model spread (1 standard deviation) from each SSP.

4 Discussion

We demonstrated the application of machine learning models, trained with seasonally decomposed features, to predict Gross Primary Productivity (GPP) at the SMEAR II station in Hyytiälä, Finland. Using a dataset of four environmental predictors—PAR, CO_2 concentration, relative humidity, and air temperature—we achieved high predictive accuracy ($R^2 \approx 0.79$–0.90). The DNN model outperformed both baseline linear regression and XGBoost models, yielding lower RMSD and MAE. To assess ecosystem responses to future climatic shifts, we retrained the DNN on monthly averaged SMEAR II data and forced the model with an ensemble of four CMIP6 models. A site-specific linear bias correction was applied to ensure the CMIP6 climate variables were comparable to station-level observations. Validation using historical CMIP6 runs confirmed that the DNN-derived estimates were largely consistent with observed station GPP. Projections across four Shared Socioeconomic Pathways (SSPs 126, 245, 370, and 585) indicate that GPP remains relatively stable across scenarios through mid-century. However, significant divergence occurs by the end of the century under high-emission scenarios (SSPs 370 and 585). Furthermore, a

https://doi.org/10.5194/egusphere-2026-3281
Preprint. Discussion started: 24 June 2026

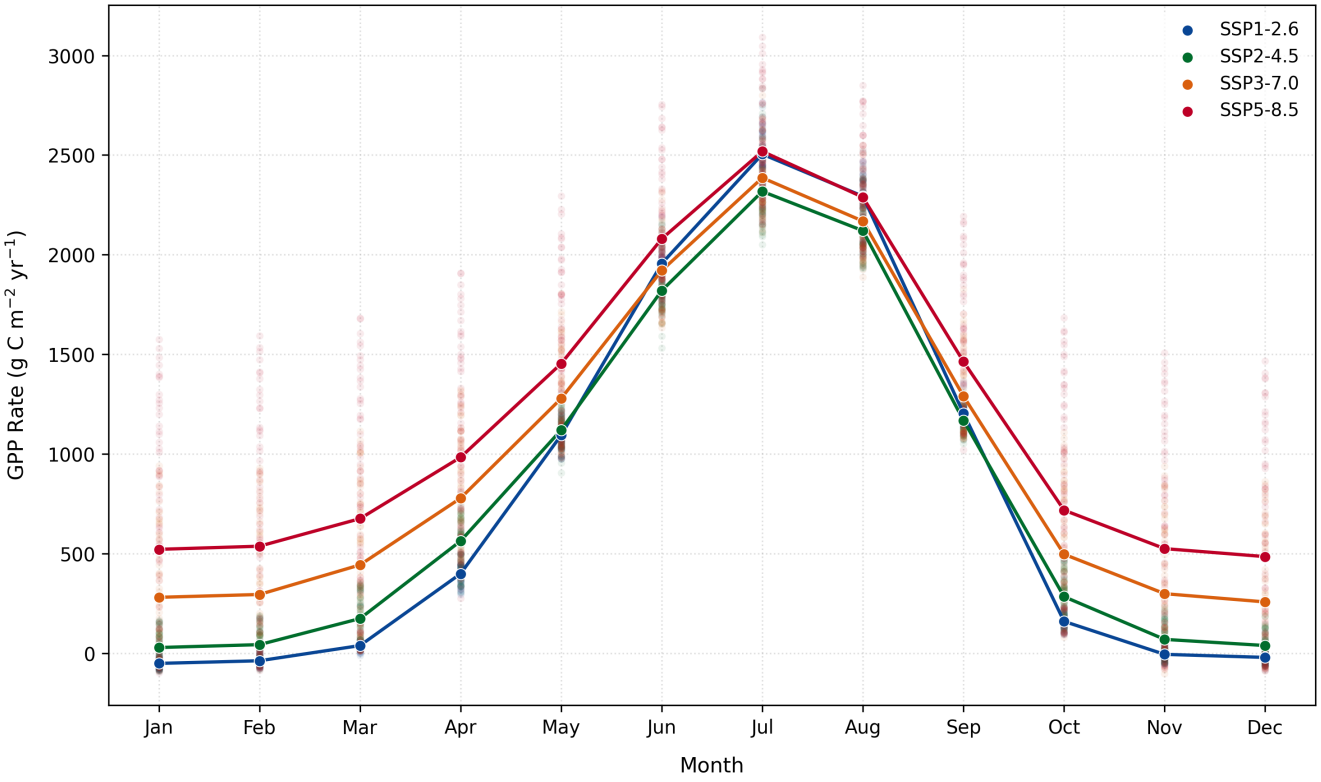

Figure 6. Projected monthly variations of GPP (2030-2100) under different CMIP6 SSPs.

monthly analysis of these projections suggests that a significant proportion of the annual GPP increase is driven by enhanced productivity during the shoulder seasons and winter months.

Our models demonstrate strong predictive performance for GPP despite using only a limited set of environmental drivers. Our best-performing model, the DNN, achieves an $R^2 \approx 0.90$ using four environmental variables and the month of the year as inputs. This is consistent with the results of Dou and Yang (2018), who estimated GPP and NEE across eight boreal and temperate forest sites in North America and Europe using four environmental drivers and a large suite of machine learning models, achieving R^2 values between 0.84–0.94 for the best-performing models across sites. Other studies have employed substantially larger feature sets while achieving comparable predictive performance. For example, Ezhova et al. (2025) used ten environmental drivers as inputs to four different machine learning models to predict NEE at the Värriö and Hyytiälä SMEAR sites, obtaining R^2 values of 0.74 and 0.90, respectively. Similarly, Cai et al. (2020) estimated NEE from sites in Scotland and the Netherlands using 22 input variables in a gradient-boosted forest model, achieving R^2 values of 0.87 and 0.90 (Cai et al., 2020). Zhu et al. (2023) predicted annual GPP from sites in China using 11 input variables across four different machine learning models, reporting R^2 values between 0.85 and 0.87 (Zhu et al., 2023). The ability to obtain strong predictive skill using a relatively small number of drivers is also supported by feature-importance studies, which suggest that dominant

https://doi.org/10.5194/egusphere-2026-3281
Preprint. Discussion started: 24 June 2026

GPP and NEE variability may be captured by a limited subset of environmental variables. For instance, Ezhova et al. (2025) identified PAR, diffuse PAR, and soil temperature as the dominant drivers of annual NEE variability, while PAR, diffuse PAR, and vapor pressure deficit were most important during the growing season. Similarly, Cai et al. (2020) found global radiation, PAR, minimum soil temperature, latent heat, and average air temperature to be among the most important predictors of NEE.

A second important aspect of the present work is the seasonal decomposition of the input variables into multiple temporal scales. Most environmental drivers exhibit strong annual periodicity, in addition to short-term fluctuations and long-term trends that may be associated with climate change. Seasonal decomposition methods are widely used in forecasting and prediction studies in the context of climate variability and climate change (Liu and Zhang, 2024; Moreno-Carbonell et al., 2020), and have also been applied to investigate GPP variability across specific temporal scales (Martínez et al., 2022; De Pue et al., 2023). In our framework, the decomposition separates each time series into seasonal, trend, and residual components, corresponding approximately to annual variability, long-term changes, and short-term fluctuations, respectively. This allows us to examine how different environmental drivers contribute to GPP variability across multiple timescales, rather than treating the signal as a single homogeneous process. We find that the residual components of the drivers contribute most strongly to GPP prediction, suggesting that short-term variability plays an important role in explaining variations in ecosystem productivity. All three trend components show comparable importance for predicted GPP, highlighting the potential relevance of long-term changes in these environmental drivers for ecosystem productivity under future climate scenarios.

Beyond predicting present-day GPP, we also estimate ecosystem productivity under future climate scenarios. While site-level GPP projections under SSP scenarios remain comparatively limited, several studies have examined future GPP changes at regional and global scales. For instance, Lu et al. (2023) studied regional average GPP over China using an ensemble of 23 CMIP6 models and reported increasing GPP trends under future climate scenarios. Similarly, Lu et al. (2024) used a CATBoost algorithm to estimate global annual GPP, projecting increases in northern mid–high latitude regions and decreases in equatorial regions. In contrast to these large-scale approaches, our framework combines site-level machine learning prediction with climate-model-driven forecasting. Specifically, we use monthly meteorological observations from the site to train machine learning models that predict GPP, and subsequently drive these trained models using station-specific bias-corrected CMIP6 projections. This provides a framework for linking local ecosystem-scale prediction with long-term climate-driven projection under different SSP pathways.

Future climate pathways, particularly high-emission scenarios (SSPs 370 and 585), force the model with input variables that lie well outside the historical training range. Despite this out-of-distribution extrapolation, our projections are directionally consistent with previous large-scale studies that report increasing GPP in cold and boreal regions under future climate scenarios. Lu et al. (2024) projected relatively modest cold-zone GPP increases by 2100, ranging from approximately 5.0% under SSP1-2.6 to 17.4% under SSP5-8.5 relative to 2021. In contrast, Knauer et al. (2023) projected substantially stronger boreal responses under RCP8.5: within the 55°N–70°N latitude band, GPP increased to roughly two- to three-fold above the 1976–2005 baseline by the end of the century, depending on the representation of photosynthetic physiology. Our site-level projections for Hyytiälä align more closely with this stronger boreal-response pattern, particularly under SSP5-8.5, where projected GPP increases from approximately 675 gC m^{-2} yr^{-1} at mid-century to 1528 gC m^{-2} yr^{-1} by end-century, corresponding to a 126% increase.

https://doi.org/10.5194/egusphere-2026-3281
Preprint. Discussion started: 24 June 2026

This study highlights three broader challenges associated with using data-driven models to project future ecosystem fluxes. First, the stochastic nature of neural network training remains a challenge, as different initializations can lead to diverging end-century outputs. While a detailed overview of this variability is provided in Appendix D, two consistent trends emerge, namely that most iterations predict stable GPP levels under low-emission scenarios, and projections remain relatively similar across SSP scenarios during the mid-century period, with stronger divergence emerging toward the end of the century. Second, the spatial scale mismatch between the SMEAR-II point measurements and the CMIP6 grid cells presents a significant challenge. While this was partially addressed through site-specific linear bias corrections, systematic differences in predicted GPP during summer and winter months remain evident in the historical simulations. This suggests that nonlinear bias correction methods may be required to better capture these seasonal extremes. Finally, the choice of model architecture presents an inherent limitation. Our current models are static and do not account for temporal dependencies or lagged effects. For instance, while transient temperature or humidity spikes may have negligible impacts on GPP, prolonged or cumulative stress can significantly impair productivity. Recurrent Neural Network (RNN) architectures such as Long Short-Term Memory (LSTM) networks may be better suited to capture these antecedent effects, which is increasingly relevant given the higher frequency of extreme climate events projected under a changing climate.

More generally, time-dependent neural network approaches have also recently been used to improve GPP estimation by integrating multiple data sources; for example, multimodal models combining site-level GPP measurements with high-resolution Sentinel-1 and Sentinel-2 satellite data have been shown to capture climate-induced productivity extremes across diverse European forest types (Montero et al., 2024).

Conclusions

The significance of this work is threefold. First, it demonstrates that machine learning methods, utilizing a limited set of engineered input variables, can achieve high accuracy in GPP prediction. Second, through the seasonal decomposition of inputs, we successfully identified specific feature components that rank as primary drivers in our models. Third, we established a robust pipeline for using CMIP6 climate projections to force models trained on site-specific data, enabling localized predictions of how forest ecosystems may respond to future climate change.

Code and data availability. The code used in this study is available at https://github.com/sgeorge91/CMIP6Studies-Forest. CMIP6 climate model data are publicly available from the Earth System Grid Federation (ESGF; https://esgf-node.llnl.gov/). Up-to-date observational data from the SMEAR II site can be accessed at https://smear.avaa.csc.fi/.

Appendix A: Seasonal Decomposition

We describe the procedure used to decompose the input environmental variables. Each variable, $Y(t)$, was represented as the sum of three additive components,

https://doi.org/10.5194/egusphere-2026-3281
Preprint. Discussion started: 24 June 2026

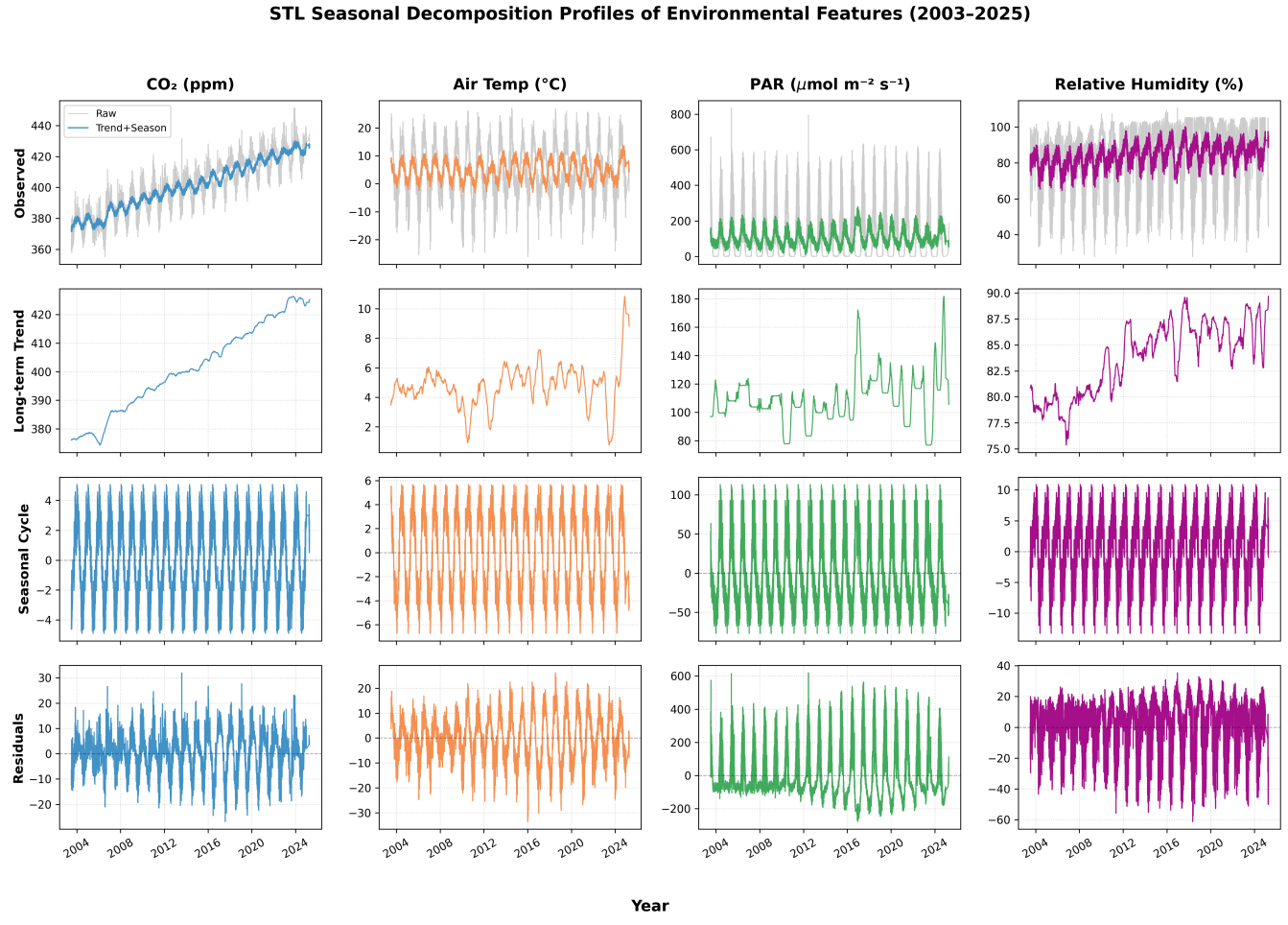

Figure A1. Decomposition of input environmental variables into trend, seasonal and residual components.

$$Y(t) = T(t) + S(t) + R(t), \tag{A1}$$

where $T(t)$ is the trend component, $S(t)$ is the seasonal component, and $R(t)$ is the residual component.

The trend component $T(t)$ was estimated using a 365-day moving average, which smooths high-frequency variability and highlights long-term changes in the time series. The seasonal component $S(t)$ was then computed by averaging the detrended series, $Y(t) - T(t)$, for each day of the year across the full observational period. Finally, the residual component $R(t)$ was obtained by subtracting the trend and seasonal components from the original time series.

Examples of the raw time series and their corresponding decomposed components are shown in Figure A1. The decomposition was performed using the `statsmodels` package.

https://doi.org/10.5194/egusphere-2026-3281
Preprint. Discussion started: 24 June 2026

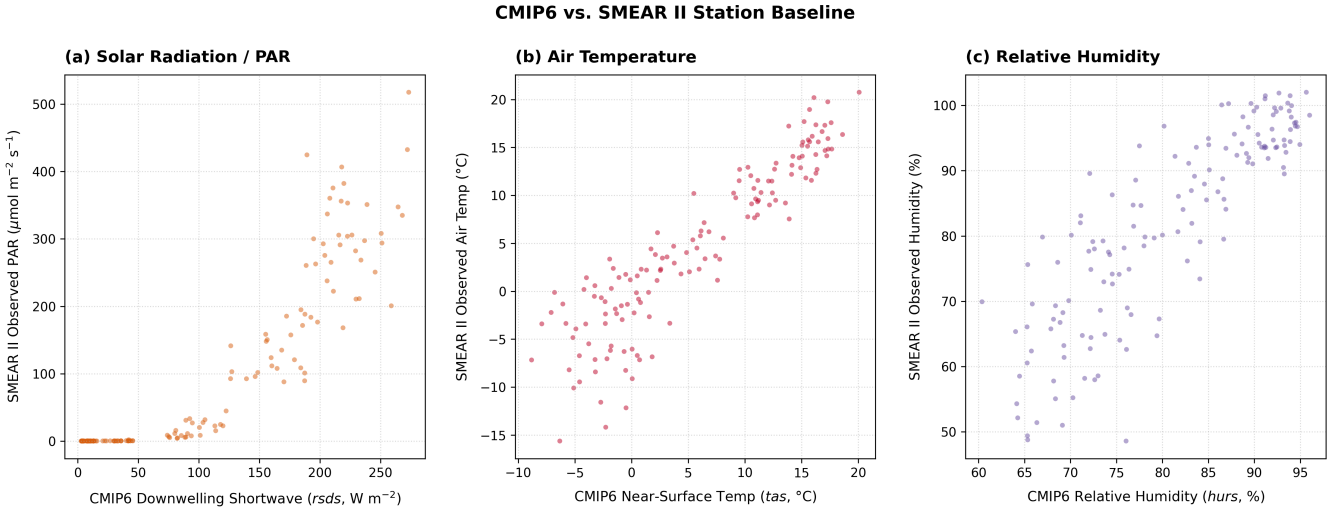

Figure B1. CESM2 historical model run vs station measurements for the same period for (a) PAR (b) AT and (c)RH.

Appendix B: Station-Specific Corrections for CMIP6 Data

To ensure consistency between the CMIP6 climate projections and observations from the SMEAR II site, we applied a station-specific bias-correction procedure to each environmental driver. Monthly observations of relative humidity (RH), air temperature (AT), and photosynthetically active radiation (PAR) were compared with the corresponding variables from the historical CMIP6 simulations over the overlapping period 2003-2014 for each of the 4 CMIP6 models. For RH and AT, a linear regression model was used to map the CMIP6 values onto the observational scale. Let Y_{site} denote the observed value at SMEAR II and Y_{CMIP} the corresponding value from the CMIP6 simulation. The relationship was assumed to be

$$Y_{\mathrm{site}} = mY_{\mathrm{CMIP}} + c, \tag{B1}$$

where m and c are the fitted slope and intercept, respectively. The fitted relationship was subsequently applied to the full CMIP6 time series to obtain bias-corrected projections.

For PAR, the same linear model was used; however, the regression coefficients were estimated only from observations satisfying $Y_{\mathrm{CMIP}} > 10$ in order to avoid fitting near-zero radiation values. The fitted relationship was then applied to the full CMIP6 time series, with negative corrected values truncated to zero to enforce the physical constraint that PAR cannot take negative values. For the CO_2 concentration, the CMIP6 values were used directly.

Examples comparing the historical CESM2 simulations with the corresponding SMEAR II observations are shown in Figure B1.

https://doi.org/10.5194/egusphere-2026-3281
Preprint. Discussion started: 24 June 2026

Appendix C: Historical runs for CMIP6 models

As described in Appendix B, the environmental drivers from the CMIP6 historical simulations are bias-corrected using a linear model fitted between site-measured variables and the corresponding CMIP6 outputs. The corrected drivers are then used as inputs to the trained machine learning models, and model performance is evaluated using Quantile–Quantile (Q–Q) plots comparing observed and predicted GPP.

The multi-model Q–Q comparison (Figure C1) shows generally good agreement in the lower range (≤ 1.5 g C m^{-2} d^{-1}) across the four evaluated GCM-driven model configurations (CESM2, EC-Earth3, NorESM2, and CNRM-CM6-1). In this range, all models closely follow the 1:1 line, indicating good representation of low GPP conditions. In the mid-range (1.5–6.0 g C m^{-2} d^{-1}), small deviations from the parity line are observed, reflecting differences in how intermediate productivity levels are reproduced across models. At higher quantiles (above the 75th percentile), all models show a consistent tendency to underestimate peak GPP values relative to observations, although the deviation remains broadly similar across the ensemble.

This suggests that the models reproduce the central distribution of GPP reasonably well, while exhibiting underestimation in the upper tail, which may lead to an under-representation of high productivity events in the simulated output.

Appendix D: Variability Across Neural Network Initializations

We investigate the uncertainty in projected GPP arising from different neural network initializations under different SSP scenarios for a single CMIP6 model, namely CESM2. The model was trained using 10 different random initializations, and the site-corrected CMIP6 drivers were used to generate projections. The ensemble median and interquartile range of the resulting predictions are shown in Figure D1.

The median projections are broadly consistent with the CMIP6 ensemble results presented in Section 3.2, exhibiting similar behaviour across scenarios. In particular, the projections remain relatively similar through mid-century before diverging towards the end of the century. The lower-emission scenarios (SSP1-2.6 and SSP2-4.5) show only modest increases in end-century GPP relative to present-day values, whereas the higher-emission scenarios (SSP3-7.0 and SSP5-8.5) produce substantially larger increases.

Author contributions. SVG: Conceptualization, Methodology, Formal Analysis, Writing – Original Draft, Writing – Review & Editing, Supervision; CTP: Conceptualization, Methodology, Formal Analysis, Writing – Original Draft; SJV: Writing – Review & Editing, Supervision; RS: Conceptualization, Writing – Review & Editing, Supervision.

Competing interests. The authors declare no competing interests.

https://doi.org/10.5194/egusphere-2026-3281
Preprint. Discussion started: 24 June 2026

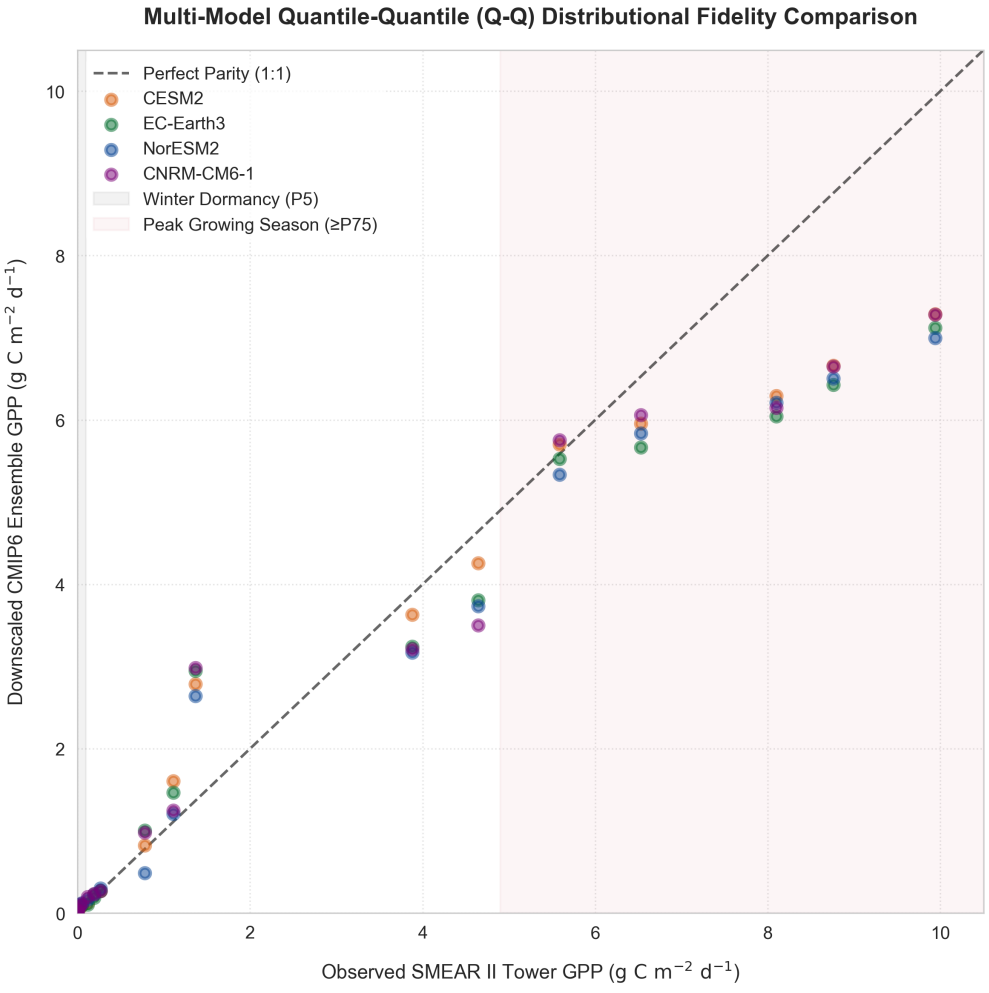

Figure C1. Quantile-Quantile plot for the GPP predicted using the drivers from the historical runs for the four CMIP6 models.

Acknowledgements. The authors acknowledge the use of Google Gemini and ChatGPT for coding assistance and language editing during manuscript preparation.

https://doi.org/10.5194/egusphere-2026-3281
Preprint. Discussion started: 24 June 2026

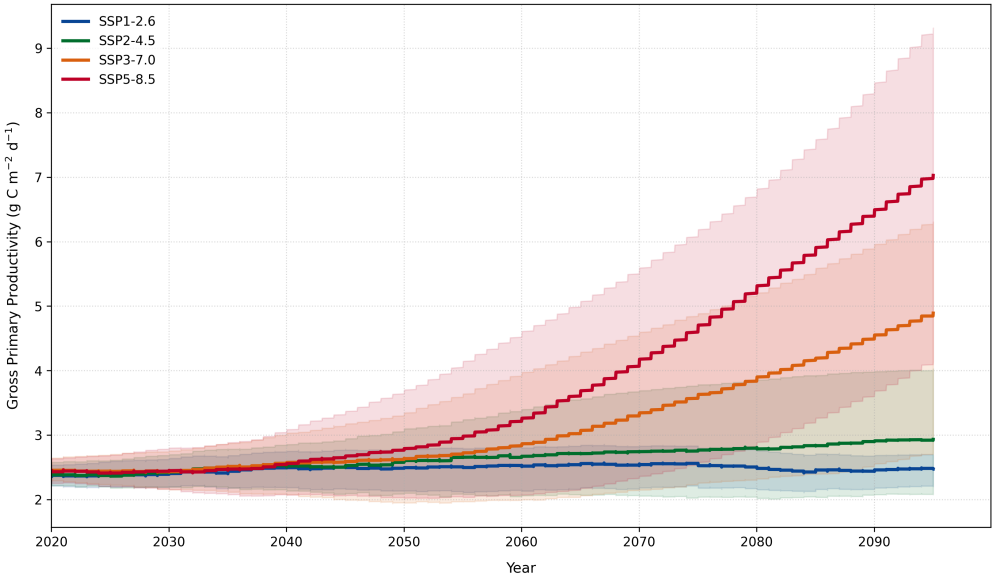

Figure D1. Temporal evolution of predictions from CESM2. The solid line shows the median prediction and shaded regions show the interquartile range for an ensemble of 10 neural network runs.

References

Abadi, M., Barham, P., Chen, J., Chen, Z., Davis, A., Dean, J., Devin, M., Ghemawat, S., Irving, G., Isard, M., et al.: {TensorFlow}: a system for {Large-Scale} machine learning, in: 12th USENIX symposium on operating systems design and implementation (OSDI 16), pp. 265–283, 2016.

Agarwal, G., Burman, P. K. D., Kulkarni, V. Y., and Kosamkar, P. K.: Prediction of Gross Primary Productivity using Hybrid LSTM-GRU Neural Networks and ERA5-Reanalysis Data, in: 2023 International Conference on Computing, Communication, and Intelligent Systems (ICCCIS), pp. 94–99, IEEE, 2023.

Agarwal, G., Burman, P., Kosamkar, P., and Kulkarni, V.: Predicting Gross Primary Productivity of the Forest Ecosystems using Machine Learning Techniques: A Review of Existing Approaches, in: IOP Conference Series: Earth and Environmental Science, vol. 1285, p. 012014, IOP Publishing, 2024.

Ahlström, A., Raupach, M. R., Schurgers, G., Smith, B., Arneth, A., Jung, M., Reichstein, M., Canadell, J. G., Friedlingstein, P., Jain, A. K., et al.: The dominant role of semi-arid ecosystems in the trend and variability of the land CO2 sink, Science, 348, 895–899, 2015.

Ashton, M. S., Tyrrell, M. L., Spalding, D., and Gentry, B.: Managing forest carbon in a changing climate, Springer Science & Business Media, 2012.

Bo, Y., Li, X., Liu, K., Wang, S., Zhang, H., Gao, X., and Zhang, X.: Three decades of gross primary production (GPP) in China: Variations, trends, attributions, and prediction inferred from multiple datasets and time series modeling, Remote Sensing, 14, 2564, 2022.

Cai, J., Xu, K., Zhu, Y., Hu, F., and Li, L.: Prediction and analysis of net ecosystem carbon exchange based on gradient boosting regression and random forest, Applied energy, 262, 114 566, 2020.

https://doi.org/10.5194/egusphere-2026-3281
Preprint. Discussion started: 24 June 2026

Chen, T. and Guestrin, C.: Xgboost: A scalable tree boosting system, in: Proceedings of the 22nd acm sigkdd international conference on knowledge discovery and data mining, pp. 785–794, 2016.

De Pue, J., Wieneke, S., Bastos, A., Barrios, J. M., Liu, L., Ciais, P., Arboleda, A., Hamdi, R., Maleki, M., Maignan, F., Gellens-Meulenberghs, F., Janssens, I., and Balzarolo, M.: Temporal variability of observed and simulated gross primary productivity, modulated by vegetation state and hydrometeorological drivers, Biogeosciences, 20, 4795–4818, https://doi.org/10.5194/bg-20-4795-2023, 2023.

de Vries, W., Du, E., and Butterbach-Bahl, K.: Short and long-term impacts of nitrogen deposition on carbon sequestration by forest ecosystems, Current Opinion in Environmental Sustainability, 9, 90–104, 2014.

Dou, X. and Yang, Y.: Estimating forest carbon fluxes using four different data-driven techniques based on long-term eddy covariance measurements: Model comparison and evaluation, Science of the Total Environment, 627, 78–94, 2018.

Ezhova, E., Laanti, T., Lintunen, A., Kolari, P., Nieminen, T., Mammarella, I., Heljanko, K., and Kulmala, M.: Explainable machine learning for modeling of net ecosystem exchange in boreal forests, Biogeosciences, 22, 257–288, 2025.

Fernández-Martínez, M., Vicca, S., Janssens, I. A., Ciais, P., Obersteiner, M., Bartrons, M., Sardans, J., Verger, A., Canadell, J., Chevallier, F., et al.: Atmospheric deposition, CO2, and change in the land carbon sink, Scientific Reports, 7, 9632, 2017.

Gauthier, S., Bernier, P., Kuuluvainen, T., Shvidenko, A. Z., and Schepaschenko, D. G.: Boreal forest health and global change, Science, 349, 819–822, 2015.

Graham, R. L., Turner, M. G., and Dale, V. H.: How increasing CO2 and climate change affect forests, BioScience, 40, 575–587, 1990.

Green, J. K., Konings, A. G., Alemohammad, S. H., Berry, J., Entekhabi, D., Kolassa, J., Lee, J.-E., and Gentine, P.: Regionally strong feedbacks between the atmosphere and terrestrial biosphere, Nature geoscience, 10, 410–414, 2017.

Hari, P., Nikinmaa, E., Pohja, T., Siivola, E., Bäck, J., Vesala, T., and Kulmala, M.: Station for measuring ecosystem-atmosphere relations: SMEAR, Physical and physiological forest ecology, pp. 471–487, 2013.

He, J., Hong, L., Shao, C., and Tang, W.: Global evaluation of simulated surface shortwave radiation in CMIP6 models, Atmospheric research, 292, 106 896, 2023.

Juho, A., Anttila, V., Kolari, P., Ilkka, K., Anna, I., Janne, L., Pauliina, S.-A., and Jaana, B.: Hyytiälä SMEAR II forest year 2020 thinning tree and carbon inventory data, https://doi.org/10.5281/zenodo.7639833, 2023.

Junninen, H., Lauri, A., Keronen, P., Aalto, P., Hiltunen, V., Hari, P., and Kulmala, M.: Smart-SMEAR: on-line data exploration and visualization tool for SMEAR stations, Boreal Environment Research, 14, 447, 2009.

Kafy, A.-A., Saha, M., Fattah, M. A., Rahman, M. T., Duti, B. M., Rahaman, Z. A., Bakshi, A., Kalaivani, S., Rahaman, S. N., and Sattar, G. S.: Integrating forest cover change and carbon storage dynamics: leveraging Google Earth Engine and InVEST model to inform conservation in hilly regions, Ecological Indicators, 152, 110 374, 2023.

Keenan, R. J., Reams, G. A., Achard, F., de Freitas, J. V., Grainger, A., and Lindquist, E.: Dynamics of global forest area: Results from the FAO Global Forest Resources Assessment 2015, Forest Ecology and Management, 352, 9–20, 2015.

Keenan, T. F., Prentice, I. C., Canadell, J. G., Williams, C. A., Wang, H., Raupach, M., and Collatz, G. J.: Recent pause in the growth rate of atmospheric CO2 due to enhanced terrestrial carbon uptake, Nature communications, 7, 13 428, 2016.

Ketkar, N. and Ketkar, N.: Introduction to keras, Deep learning with python: a hands-on introduction, pp. 97–111, 2017.

Knauer, J., Cuntz, M., Smith, B., Canadell, J. G., Medlyn, B. E., Bennett, A. C., Caldararu, S., and Haverd, V.: Higher global gross primary productivity under future climate with more advanced representations of photosynthesis, Science Advances, 9, eadh9444, 2023.

https://doi.org/10.5194/egusphere-2026-3281
Preprint. Discussion started: 24 June 2026

Kulmala, L., Pumpanen, J., Kolari, P., Dengel, S., Berninger, F., Köster, K., Matkala, L., Vanhatalo, A., Vesala, T., and Bäck, J.: Inter-and intra-annual dynamics of photosynthesis differ between forest floor vegetation and tree canopy in a subarctic Scots pine stand, Agricultural and Forest Meteorology, 271, 1–11, 2019.

Launiainen, S., Katul, G. G., Lauren, A., and Kolari, P.: Coupling boreal forest CO2, H2O and energy flows by a vertically structured forest canopy–Soil model with separate bryophyte layer, Ecological modelling, 312, 385–405, 2015.

Launiainen, S., Katul, G. G., Leppä, K., Kolari, P., Aslan, T., Grönholm, T., Korhonen, L., Mammarella, I., and Vesala, T.: Does growing atmospheric CO2 explain increasing carbon sink in a boreal coniferous forest?, Global Change Biology, 28, 2910–2929, 2022.

LeCun, Y., Bengio, Y., and Hinton, G.: Deep learning, nature, 521, 436–444, 2015.

Liu, X. and Zhang, Q.: Combining seasonal and trend decomposition using LOESS with a gated recurrent unit for climate time series forecasting, IEEE Access, 12, 85 275–85 290, 2024.

Loescher, H., Law, B., Mahrt, L., Hollinger, D., Campbell, J., and Wofsy, S.: Uncertainties in, and interpretation of, carbon flux estimates using the eddy covariance technique, Journal of Geophysical Research: Atmospheres, 111, 2006.

Lu, J., Wang, G., Feng, D., and Nooni, I. K.: Improving the gross primary production estimate by merging and downscaling based on deep learning, Forests, 14, 1201, 2023.

Lu, Q., Liu, H., Wei, L., Zhong, Y., and Zhou, Z.: Global prediction of gross primary productivity under future climate change, Science of the Total Environment, 912, 169 239, 2024.

Martínez, B., Sánchez-Ruiz, S., Campos-Taberner, M., García-Haro, F. J., and Gilabert, M. A.: Exploring ecosystem functioning in Spain with gross and net primary production time series, Remote Sensing, 14, 1310, 2022.

Mercado, L. M., Bellouin, N., Sitch, S., Boucher, O., Huntingford, C., Wild, M., and Cox, P. M.: Impact of changes in diffuse radiation on the global land carbon sink, Nature, 458, 1014–1017, 2009.

Montero, D., Mahecha, M. D., Martinuzzi, F., Aybar, C., Klosterhalfen, A., Knohl, A., Koebsch, F., Anaya, J., and Wieneke, S.: Recurrent Neural Networks for Modelling Gross Primary Production, arXiv preprint arXiv:2404.12745, 2024.

Moreno-Carbonell, S., Sanchez-Ubeda, E. F., and Munoz, A.: Time series decomposition of the daily outdoor air temperature in Europe for long-term energy forecasting in the context of climate change, Energies, 13, 1569, 2020.

O'Neill, B. C., Tebaldi, C., Van Vuuren, D. P., Eyring, V., Friedlingstein, P., Hurtt, G., Knutti, R., Kriegler, E., Lamarque, J.-F., Lowe, J., et al.: The scenario model intercomparison project (ScenarioMIP) for CMIP6, Geoscientific Model Development, 9, 3461–3482, 2016.

Palmer, T. E., McSweeney, C. F., Booth, B. B., Priestley, M. D., Davini, P., Brunner, L., Borchert, L., and Menary, M. B.: Performance-based sub-selection of CMIP6 models for impact assessments in Europe, Earth System Dynamics, 14, 457–483, 2023.

Pysarenko, L., Krakovska, S., Savenets, M., Ezhova, E., Lintunen, A., Petäjä, T., Bäck, J., and Kulmala, M.: Two-decade variability of climatic factors and its effect on the link between photosynthesis and meteorological parameters: example of Finland's boreal forest, Boreal Environment Research, 27, 1, 2022.

Sarkar, D. P., Shankar, B. U., and Parida, B. R.: Machine learning approach to predict terrestrial gross primary productivity using topographical and remote sensing data, Ecological Informatics, 70, 101 697, 2022.

Seabold, S. and Perktold, J.: Statsmodels: econometric and statistical modeling with python., SciPy, 7, 2010.

Tebaldi, C., Debeire, K., Eyring, V., Fischer, E., Fyfe, J., Friedlingstein, P., Knutti, R., Lowe, J., O'Neill, B., Sanderson, B., et al.: Climate model projections from the scenario model intercomparison project (ScenarioMIP) of CMIP6, Earth System Dynamics, 12, 253–293, 2021.

https://doi.org/10.5194/egusphere-2026-3281
Preprint. Discussion started: 24 June 2026

Thrasher, B., Wang, W., Michaelis, A., Melton, F., Lee, T., and Nemani, R.: NASA global daily downscaled projections, CMIP6, Scientific data, 9, 262, 2022.

Walker, J. C. and Kasting, J. F.: Effects of fuel and forest conservation on future levels of atmospheric carbon dioxide, Global and planetary change, 5, 151–189, 1992.

Yang, F., Ichii, K., White, M. A., Hashimoto, H., Michaelis, A. R., Votava, P., Zhu, A.-X., Huete, A., Running, S. W., and Nemani, R. R.: Developing a continental-scale measure of gross primary production by combining MODIS and AmeriFlux data through Support Vector Machine approach, Remote Sensing of Environment, 110, 109–122, 2007.

Zhu, N., Liu, C., Laine, A. F., and Guo, J.: Understanding and Modeling Climate Impacts on Photosynthetic Dynamics with FLUXNET Data and Neural Networks, Energies, 13, 1322, 2020.

Zhu, X.-J., Yu, G.-R., Chen, Z., Zhang, W.-K., Han, L., Wang, Q.-F., Chen, S.-P., Liu, S.-M., Wang, H.-M., Yan, J.-H., et al.: Mapping Chinese annual gross primary productivity with eddy covariance measurements and machine learning, Science of the Total Environment, 857, 159 390, 2023.